

Polarons and Bipolarons in Holstein and Holstein $t - J$ models by Dynamical Mean Field Theory

S. CIUCHI⁽¹⁾, M. CAPONE⁽²⁾, E. CAPPELLUTI⁽²⁾ AND G. SANGIOVANNI⁽³⁾

⁽¹⁾ *Dipartimento di Fisica Università dell'Aquila, via Vetoio, I-67010 Coppito-L'Aquila, Italy*

⁽²⁾ *"Istituto dei Sistemi Complessi", CNR-INFN, v. dei Taurini 19, 00185 Roma, Italy,*

⁽³⁾ *Max-Planck Institut für Festkörperforschung, Heisenbergstr. 1, D-70569 Stuttgart, Germany*

1. – Introduction

In system with strong electron-phonon (e-ph) interaction, the carriers lose mobility, ultimately acquiring polaronic character. A polaron is a state in which the phonon and electron degrees of freedom are strongly entangled, and the presence of an electron is associated to a finite lattice distortion, which in turn binds the electron leading to the so-called self-trapping effect. Polarons also tend to create bound pairs, called bipolarons of course the presence of Coulomb repulsion destabilize bi-polarons in favor of a pure polaronic state at finite densities [1, 2]. Typical signatures of polarons are seen in multi-peaked photoemission spectra[3] and transport measurements, where an activated behavior with a characteristic energy given by the polaronic binding energy is observed. The polaronic peak found in the mid infrared measurements of optical conductivity [4] may also not only detect the polaronic binding energy [5] but also other subtle polaronic transitions at very low energy [6]. Another less classical indication of polaronic formation comes from the analysis of lattice displacements associated to the excess charge as obtained by the distribution of distances between atoms[3].

A joint analysis of both spectral [5] and local lattice distortions can disentangle various kind of behavior in polaronic systems. In fact we notice that neglecting the repulsive interaction a gapped pair state can be formed even without a significant associated polarization. In this case bipolarons are expected to be a relatively mobile particle.

The aim of this work is to provide a thorough analysis of polaronic spectral properties in both single and multi-polaron cases. The backbone of our presentation is the DMFT which is introduced and briefly discussed in general in section 2.

In the single polaron case we review the exact solution of the Holstein model [7, 8] (section 4) and we present some new results for the Holstein $t - J$ model comparing our results with those of Mishchenko [9]. At large polaronic densities we use both Exact Diagonalization (ED) and Quantum Monte Carlo (QMC) techniques to solve the DMFT equations for the Holstein model respectively at the $T = 0$ (sec. 5) and $T > 0$ (section 6). In this case we compare spinless and spinful fermions cases and we discuss in detail the role of the adiabatic ratio. In this way the properties of a pure polaronic state can be disentangled from those of bipolaronic state. We compare also numerical solutions

with analytic approximate schemes based on Born Oppenheimer (5.1) and Lang-Firsov canonical transformation (5.2) respectively in adiabatic and antiadiabatic regime.

2. – The DMFT method

2.1. Introduction. – Dynamical Mean Field Theory is a non-perturbative technique originally developed as the exact solution of a interacting electron problem on an infinite dimensional lattice [10, 11]. A comprehensive review can be found in ref. [12] now let us sketch some key point to understand the developments presented in following sections. Let us consider a general tight-binding problem on a lattice with coordination number z

$$(1) \quad H = -\frac{t}{\sqrt{z}} \sum_{\langle ij \rangle \sigma} c_i^\dagger c_j + \sum_i V[c_i, c_i^\dagger]$$

where c_i are fermionic annihilation operator acting on site i (spin index omitted for simplicity) V is a local (on-site) potential. The scaling of hopping t is such as the limit $z \rightarrow \infty$ give a non trivial result. Mean field theory turns out to be exact in infinite dimensions i.e. when the number of nearest neighbor diverges, therefore we can replace the effect of hopping on neighboring sites as *cavity field* η

$$\eta_i = \frac{t}{\sqrt{z}} \sum_j^{(i)} c_j$$

with the sum running on nearest neighbor of site i . In terms of the internal fields η , Hamiltonian can be written formally as a sum of single site operators as

$$(2) \quad H = - \sum_i \eta_i^\dagger c_i - \sum_i c_i^\dagger \eta_i + \sum_i V[c_i, c_i^\dagger]$$

For fermions η obeys anticommutation relations

$$[\eta_i \eta_j^\dagger] = t \delta_{i,j} [\eta_i c_j^\dagger] = \frac{t}{\sqrt{z}} \delta_{i,j}.$$

On a more formal ground it can be demonstrated that the cavity field is a Gaussian Grassmann field which is therefore determined solely by its correlation function[12].

2.2. Single impurity action. – The previous arguments can be more formally developed using a path-integral formalism. In analogy with classical mean-field[12], the fermions of all sites but one (namely 0) are integrated out leading to a single-site partition function

$$(3) \quad Z = \int \Pi_i \mathcal{D}\psi^\dagger \mathcal{D}\psi \exp(-S)$$

where now ψ and ψ^\dagger are Grassmann anticommuting eigenvalues of the creation/destruction operators of site 0[13]. The action S is given by

$$(4) \quad S = - \int_0^\beta d\tau \int_0^\beta d\tau' \psi^\dagger(\tau) \mathcal{G}_0^{-1}(\tau - \tau') \psi(\tau') + \int_0^\beta d\tau V[\psi(\tau), \psi^\dagger(\tau)]$$

where the correlator $\mathcal{G}_0^{-1}(\tau - \tau')$ is

$$(5) \quad \mathcal{G}_0^{-1}(\tau - \tau') = \partial_\tau \delta(\tau - \tau') + \langle \eta_i(\tau) \eta_i(\tau') \rangle$$

which is independent on i due to translation invariance. The action (4) depends parametrically on the environment through the correlator \mathcal{G}_0 . (4) is indeed the action of a *single* impurity embedded in a medium whose properties are related to the original lattice via the self-consistency equation (5). To be more concrete let us consider an infinite coordination Bethe lattice of half-bandwidth D , for which the Green's function of η is proportional to the local Green's function $G_{j,j}$ [12]

$$\langle \eta_i(\tau) \eta_i(\tau') \rangle = \frac{D^2}{4z} \sum_j G_{j,j}$$

then Eq. (5) reads $\mathcal{G}_0^{-1}(\tau) = -\partial_\tau + (D^2/4)G(\tau)$, or in frequency domain

$$(6) \quad \mathcal{G}_0^{-1}(i\omega_n) = i\omega_n + (D^2/4)G(i\omega_n).$$

Eqs (3) and (4), together with the self-consistency condition (6) form a closed set of mean-field equations.

2.3. Single impurity Hamiltonian. – A Hamiltonian formalism can be also developed when suitably defined fermion fields are introduced to get required gaussian cavity field. Eq. (4) can be obtained by integrating out auxiliary fermionic fields c_k of an Anderson Impurity Hamiltonian (AIM)

$$(7) \quad H_{AIM} = \sum_k V_k (f^\dagger c_k + c_k f^\dagger) + \sum_k E_k c_k^\dagger c_k + V[f, f^\dagger]$$

levels E_k and hybridization constants V_k must be chosen to give the appropriate cavity field. In the Bethe lattice case

$$(8) \quad \frac{D^2}{4}G(i\omega_n) = \sum_k \frac{V_k^2}{i\omega_n - E_k}.$$

where in the l.h.s. we read the local *lattice* propagator. Eq. (8) becomes the self-consistency condition which determines the appropriate AIM parameters E_k and V_k .

3. – Holstein model in infinite dimensions

The Holstein molecular crystal model is the paradigmatic model for small polarons. Its Hamiltonian reads

$$(9) \quad H = -t \sum_{\langle i,j \rangle, \sigma} (c_{i,\sigma}^\dagger c_{j,\sigma} + h.c.) - g \sum_{i,\sigma} (n_{i,\sigma} - \frac{1}{2})(a_i + a_i^\dagger) + \omega_0 \sum_i a_i^\dagger a_i,$$

where $c_{i,\sigma}$ ($c_{i,\sigma}^\dagger$) and a_i (a_i^\dagger) are, respectively, destruction (creation) operators for fermions and for local vibrations of frequency ω_0 on site i , $n_{i,\sigma} = c_{i,\sigma}^\dagger c_{i,\sigma}$ the electron density per spin, t is the hopping amplitude, g is an electron phonon coupling. In the half-filled case we always fix the chemical potential to the particle-hole symmetric value, which fixes the density per spin to $n = 1/2$. In the spinless case there is no sum on σ . We choose as parameter of the model the e-ph coupling constant $\lambda = 2g^2/\omega_0 D$ where D is the half-bandwidth of our infinite-coordination Bethe lattice, and the adiabatic ratio $\gamma = \omega_0/D$. In the single electron case the spin index is unessential, moreover the mean density is zero and the el-ph interaction in Eq. (9) is replaced by $-g \sum_i n_i (a_i + a_i^\dagger)$. The partition function (3) is now defined as

$$(10) \quad Z = \int \mathcal{D}x(\tau) \int \mathcal{D}\psi^\dagger \mathcal{D}\psi(\tau) \exp(-S)$$

where using units where the spring constant $K = M\omega_0^2 = 1$ $x(\tau) = \sqrt{\omega_0/2}(a(\tau) + a^\dagger(\tau))$.

The single impurity action S associated to the lattice Hamiltonian (9) in an infinite coordination lattice reads this case:

$$(11) \quad S = - \int_0^\beta d\tau \int_0^\beta d\tau' \sum_\sigma \psi_\sigma^\dagger(\tau) \mathcal{G}_0^{-1}(\tau - \tau') \psi_\sigma(\tau') +$$

$$(12) \quad + \frac{1}{2} \int_0^\beta d\tau \left(\frac{\dot{x}^2(\tau)}{\omega_0^2} + x^2(\tau) \right) +$$

$$(13) \quad + \sqrt{\lambda} \int_0^\beta d\tau x(\tau) (n(\tau) - 1).$$

where $n(\tau) = \sum_\sigma \psi_\sigma^\dagger(\tau) \psi_\sigma(\tau)$.

3.1. DMFT-QMC method. – An efficient method to solve Eqs. (11,12,13) at finite temperature is the QMC method (in the Blankenbecler-Scalapino-Sugar approach[14]). This method works well for not too low temperatures and naturally yields electronic and bosonic correlation functions, as well as the probability distributions associated to the phonon fields. The method is not affected by the negative sign-problem, and its main limitation comes in the adiabatic regime ($\gamma \ll 1$) where the phonon becomes heavy making more difficult to sample correctly the available phase space. In the BSS scheme the fermions are integrated out, and the phonons coordinates $x(\tau)$ are discretized in L imaginary-time slices of width $\Delta\tau = \beta/L$ and then sampled by QMC. L has to be chosen large enough to reduce as much as possible $\Delta\tau$, which controls the Trotter discretization error. To keep $\Delta\tau$ less than $1/8$ we used 32 slices except for the lowest temperature ($\beta = 8$) for which we have used $L = 64$,

3.2. DMFT-ED method. – The Anderson Impurity Model for the Holstein model reads

$$(14) \quad H_{AIM} = - \sum_{k,\sigma} V_k (c_{k,\sigma}^\dagger f_\sigma + h.c.) + \sum_{k,\sigma} E_k c_{k,\sigma}^\dagger c_{k,\sigma} - \\ - g \sum_\sigma \left(f_\sigma^\dagger f_\sigma - \frac{1}{2} \right) (a + a^\dagger) + \omega_0 a^\dagger a.$$

We solve (14) by means of ED by truncating the sums in the first two terms of Eq. (14) to a small number of terms N_b , so that the Hilbert space is small enough to use, e.g., the Lanczos algorithm to compute the $T = 0$ Green's function. For the case of phonon degrees of freedom we consider here, also the infinite phonon space has to be truncated allowing for a maximum number of excited phonons N_{ph} . In all the calculations presented here the convergence of both truncations have been checked. The value of N_{ph} has to be chosen with special care in the adiabatic regime and in strong coupling, where phonon excitations are energetically convenient. As far as the discretization of the bath is concerned, the convergence of thermodynamic averages and Matsubara frequency properties is exponentially fast and $N_b \sim 8 - 9$ is enough to obtain converged results. The method also offers the advantage of a direct evaluation of real-frequency spectral properties such as the electron and phonon spectral functions. The main limitation is that these quantities reflect the discrete nature of our system. In practice, the spectra are formed by collections of δ -functions, which limits our frequency resolution, and makes the method better suited to gain knowledge on the main features of the spectra, rather than on the fine details.

3.3. Quantities of interest. – We mainly characterized electronic and phononic properties by considering respectively the electron density of states $\rho(\omega) = -\frac{1}{\pi}G(\omega)$ and the phonon probability distribution function (PDF) $P(x) = \langle \phi_0 | x \rangle \langle x | \phi_0 \rangle$, where $|x\rangle$ is a phonon coordinate eigenstate, and $|\phi_0\rangle$ is the ground state vector. At finite electron density a lattice polarization reflects in the presence of two peaks in $P(x)$, corresponding to opposite polarization of occupied and unoccupied sites (bimodal behavior) [15]. In the single electron case the polarization of a lattice site where one electron sits is a marker of a polaronic crossover. Also in this case a bimodal behavior can be observed in the adiabatic regime but generally speaking we have a definite polarization when phonon fluctuations are less than the average polarization due to the presence of the electron. In this way a *qualitative* difference is identified between the polarized and unpolarized regimes, which allows for an unambiguous way to draw a crossover line, as opposed to estimates based on smoothly varying functions as average lattice fluctuations or electron kinetic energy.

A Metal to Insulator Transition (MIT) can be probed by the low energy behavior of ρ . This is a consequence of the infinite dimensional limit where the self-energy is momentum-independent. Thus the vanishing of the low-energy quasi-particle spectral weight coincides with the divergence of the effective mass, which determines the MIT.

4. – Single electron in Holstein and Holstein t - J models

4.1. $T = 0$ continued fraction for a single polaron. – The single electron case in both Holstein, $t - J$ and $t - J$ -Holstein case can be solved semi-analytically taking advantage of peculiar features of the zero density case. We briefly describe here the formalism at $T = 0$. Generalization to thermalized lattice can be found in [8]. We use here the AIM formalism of eq. (14). For a single electron the Green's function is purely retarded, then the retarded impurity propagator can be defined as

$$(15) \quad G(\omega) = \langle 0 | f \frac{1}{\omega + i\delta - H} f^\dagger | 0 \rangle$$

which has the correct prescription $\delta > 0$ for convergence of the time integrals. The vacuum energy is defined here to be zero. To proceed further one needs to introduce the

generalized matrix elements

$$(16) \quad G_{n,m} = \langle 0 | \frac{a^n}{\sqrt{n!}} f \frac{1}{\omega + i\delta - H} f^\dagger \frac{(a^\dagger)^m}{\sqrt{m!}} | 0 \rangle$$

so that the element $G_{0,0}$ will be the Green function.

Let us separate the impurity Hamiltonian of eq. (14) into H_0 and H_I , H_I is the local interaction term and H_0 the remainder. A useful operator identity for the resolvent is

$$(17) \quad \frac{1}{z - H} = \frac{1}{z - H_0} + \frac{1}{z - H_0} H_I \frac{1}{z - H}$$

The diagonal matrix element of this operator on the impurity zero phonon state $f^\dagger | 0 \rangle$ is the Green's function of eq. (15).

In the subspace of zero electron p -phonon states $| 0, p \rangle = (a^\dagger)^p / \sqrt{p!} | 0 \rangle$ one can write

$$(18) \quad H_I = \sum_p f^\dagger | 0, p \rangle \langle 0, p | f (a + a^\dagger)$$

leading to the recursion formula for the $G_{n,m}$'s

$$(19) \quad G_{n,m} = G_{0n} \delta_{n,m} - g \sum_p G_{0n} X_{n,p} G_{p,m}$$

where $G_{0n} = G_0(\omega - n\omega_0)$ is the diagonal element of the free resolvent and $X_{n,p}$ are the phonon displacement matrix elements $X_{n,p} = \sqrt{p+1} \delta_{n,p+1} + \sqrt{p} \delta_{n,p-1}$.

One immediately recognizes that, due to the particular form of the matrix \mathbf{X} , \mathbf{G}^{-1} is a tridiagonal matrix, so that the solution of the problem is reduced to the inversion of a matrix in arbitrary dimensions. Following the lines given in Ref.[16] one can express the diagonal element of the \mathbf{G} matrix in terms of the diagonal and non-diagonal elements of \mathbf{G}^{-1} . The local propagator (the 0,0 element of \mathbf{G}) is obtained in terms of a Continued Fraction Expansion (CFE), as a functional of the "bare" propagator G_0 :

$$(20) \quad G(\omega) = \frac{1}{G_0^{-1}(\omega) - \frac{g^2}{G_0^{-1}(\omega - \omega_0) - \frac{2g^2}{G_0^{-1}(\omega - 2\omega_0) - \frac{3g^2}{G_0^{-1}(\omega - 3\omega_0) - \dots}}}}$$

Due to the impurity analogy, this is also the local propagator of the original lattice problem, provided that self-consistency condition (eq. (6) for real frequencies) is fulfilled. As a consequence the lattice self-energy Σ is immediately obtained by $G = 1/(G_0^{-1} - \Sigma)$. An example of the spectral function that can be obtained with this formalism is presented also in this volume (see [17] fig. 4).

4.2. *Holstein $t - J$ model in infinite dimensions.* – To derive the Holstein- $t - J$ Hamiltonian for a single hole we sketch the treatment of Ref. [18]. First the $t - J$ Hamiltonian is transformed by a canonical transformation into a ferromagnetic one. Then we introduce fermionic h hole and bosonic b spin-defect on the antiferromagnetic ground state operators. As a further step an Holstein-Primakoff transformations is performed which introduces spin waves [19], then we adopt the linear spin wave scheme and we use explicitly the infinite coordination limit to get:

$$(21) \quad H = \frac{t}{2\sqrt{z}} \sum_{\langle ij \rangle \sigma} \left(h_j^\dagger h_i a_j + \text{h.c.} \right) - g \sum_i \left[h_i^\dagger h_i - \langle h_i^\dagger h_i \rangle \right] (a_i + a_i^\dagger) + \omega_0 \sum_i a_i^\dagger a_i + \frac{J}{4z} \sum_{\langle ij \rangle} \left[b_i^\dagger b_i + b_j^\dagger b_j \right] + \frac{J}{2} \sum_i h_i^\dagger h_i.$$

The first term of Eq. (21) describe the kinetic hopping of one hole on the antiferromagnetic background, which is accompanied by the creation (destruction) of a spin defect which breaks (restores) $2z$ magnetic bonds with individual energy $J/4z$. In addition we have the usual local e-ph interaction which couples the hole density to the local phonon. The last term in Eq. (21) can be absorbed in the definition of the hole chemical potential which, for the single hole case here considered, has to be set at the bottom of the hole band. The single-hole Green's function is given by the resolvent of Eq. (15) in which the spinless fermions f are replaced now by the hole operators h . Following the same path of the previous calculation and using the results of Ref. [20] for the $t - J$ model, we can write the local hole propagator $G(\omega)$ as function of the sum of a hopping and a phonon contribution to the self-energy[18]:

$$(22) \quad G(\omega) = \frac{1}{\omega - \Sigma_{\text{hop}}(\omega) - \Sigma_{\text{el-ph}}(\omega)},$$

where the hopping contribution describes the dynamics of the hole through the antiferromagnetic background,

$$(23) \quad \Sigma_{\text{hop}}(\omega) = \frac{t^2}{4} G(\omega - J/2),$$

while the e-ph self-energy takes into account the on site multiple scattering with phonons and it is formally the same as in Eq. (20) after identifying

$$(24) \quad G_0^{-1}(\omega) = \omega - \frac{t^2}{4} G(\omega - J/2).$$

Both $\Sigma_{\text{hop}}(\omega)$ and $\Sigma_{\text{el-ph}}(\omega)$ are expressed as functionals of the *total* Green's function $G(\omega)$ leading to a self-consistent interplay between the spin and the e-ph interaction. Eqs. (22), (23) and (24) represent a closed self-consistent system which we can be numerically solved by iterations to obtain the explicit *exact* expression of the local Green's function $G(\omega)$ [18]. The formal scheme looks quite similar to the single electron solution of the Holstein model [8]. However, due to the antiferromagnetic background, the physical interpretation is quite different.

Due to the orthogonality of the initial and final antiferromagnetic background, the non-local component of the Green's function in the Holstein- $t - J$ model, even for $J = 0$, is

strictly zero $G_{ij}(\omega) = G(\omega)\delta_{ij}$, [20] whereas for the pure Holstein model $G_{i\neq j}(\omega)$ is finite and provides informations about the non-local dynamics: $G(\mathbf{k}, \omega) = 1/[\omega - \epsilon_{\mathbf{k}} - \Sigma(\omega)]$.

In addition, the magnetic ordering has important consequences also on the local Green's function $G_{ii}(\omega)$. In the pure Holstein model for instance $G_{ii}(\omega)$ takes into account any generic dynamics which occurs back and forth a given site whereas in the Holstein- t - J model the electron must follow a retraceable path in order to restore the antiferromagnetic background. [20] A Bethe-like dynamics is thus enforced by the magnetic ordering regardless the actual real space lattice. The object made up by the hole plus the local modification of the spin configuration due to the presence of the hole is the "spin polaron".

4.3. Results. – The local physical properties of one hole in the infinite dimension Holstein- t – J model have been extensively investigated in Ref. [18]. In Fig. 1 we report the evolution of the local spectral function $\rho(\omega) = -(1/\pi)\text{Im}G(\omega)$ as function of the spin-exchange J/t and of the e-ph interaction λ for $\omega_0/t = 0.1$. In the limits $J = 0$ and

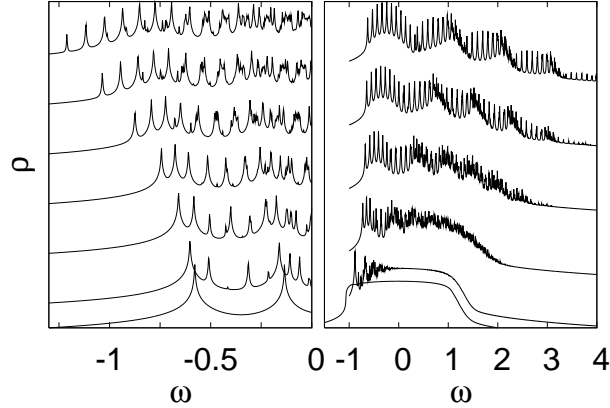


Fig. 1. – Hole spectral function in the t – J -Holstein model for $\gamma = 0.1$ as function of J/t and λ . Left panel: $J/t = 0.4$ and (from bottom to top) $\lambda = 0.0, 0.05, 0.15, 0.25, 0.35, 0.45, 0.55$. Right panel: $\lambda = 0.25$ and (from bottom to top) $J/t = 0.0, 0.1, 0.5, 1.0, 1.5, 2.0$.

$\lambda = 0$ we recover respectively the results of Refs. [8] and [20]. They are qualitatively different: for $J/t = 0$ and finite λ the spectral density is the same as the pure Holstein model (see e.g. fig. 5 [17] of the present volume), whereas for $\lambda = 0$ and finite J/t the spectrum is described by magnetic peaks spaced as $(J/t)^{2/3}$ (for small J/t). Switching on at the same time both the magnetic interaction and the e-ph interaction gives rise to the interesting interplay between these degrees of freedom. This can be shown for instance in the evolution of the spectral function as function of λ : increasing the e-ph interaction not only gives rise to additional phonon peaks which superimpose on the magnetic one, but it also enhances the nature of the magnetic polaron, from a large one (corresponding to $(J/t)^{2/3}$ spaced peaks) to a more localized one (corresponding to (J/t) spaced peaks). A similar behavior appears as function of J/t : here for large J/t the gross structure of the spectral function is described by equally (J) spaced magnetic structures with fine features determined by the e-ph interaction. Note that this latter is represented by phononic peaks spaced by ω_0 as in the antiadiabatic limit, although γ here is just

$\gamma = 0.1$, since the antiadiabatic regime is intrinsically enforced by the reduction of the kinetic energy due to the magnetic polaron trapping. In any case within DMFT we loose hole band dispersion. As a consequence we were not able to reproduce even qualitatively the interchange of magnetic and polaronic peaks observed by increasing el-ph coupling at finite dimensionality [9]. However within our localized solution we recover many of the qualitative features of both magnetic and lattice polaron crossovers [18].

Another interesting quantity which points out the interplay between magnetic and e-ph interaction is the PDF $P(x)$. Notice due to localization of DMFT solution $P(x)$ gives the lattice distortion associated to the localization center. In the left panel of Fig. 2 we show the $P(x)$ for $J/t = 0.4$ as function of λ . Here the lattice polaron formation

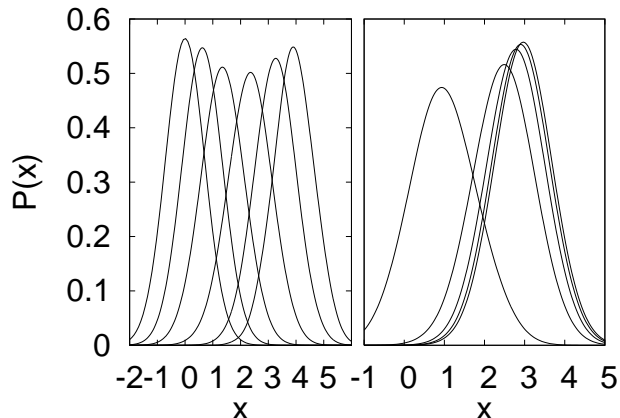


Fig. 2. – Phonon PDF in the t – J -Holstein model for $\omega_0/t = 0.5$ Left panel: $J/t = 0.4$ and (from left to right) $\lambda = 0.0, 0.05, 0.25, 0.5, 0.75, 1.0, 1.25$. Right: $\lambda = 0.5$ from left to right $J/t = 2.0, 1.0, 0.4, 0.05$.

is characterized by the value λ_{pol} at which broadening of the PDF is maximum. For larger λ the PDF recovers a gaussian form due to the lattice fluctuations around the new minima at finite distortion. The magnetic polaron formation is also pointed out by the analysis of the $P(x)$ (right panel of Fig. 2): the magnetic trapping favors the lattice one, further reducing the anomalous lattice fluctuations towards the gaussian ones.

5. – Half-filled Holstein model: spinless vs spinful cases at $T = 0$

5.1. Adiabatic regime. – We briefly describe, as a starting point of the Born-Oppenheimer (BO) procedure, the adiabatic limit in which $\gamma \rightarrow 0$ keeping λ fixed. This limit has been thoroughly studied in Ref. [15] which we here briefly resume. When $\omega_0 \rightarrow 0$ and λ finite the kinetic term (12) forces the phonon path $x(\tau)$ to be τ -independent, $x(\tau) \equiv x$. Phonons becomes classical and the interaction term reads $-\sqrt{\lambda}x \int_0^\beta d\tau (n(\tau) - 1)$. The gaussian integrals in (10) with the action given by (11,12,13) can be computed analytically leading to

$$(25) \quad Z = \int dx \exp(-\beta V(x))$$

where the adiabatic potential $V(x)$ is [21, 10, 22]

$$(26) \quad V(x) = \frac{1}{2}x^2 - \frac{\sqrt{\lambda}}{2}|x| - \frac{s}{\beta} \sum_n \log \left(\frac{G_0^{-1}(i\omega_n) + \sqrt{\lambda}x}{i\omega_n + \sqrt{\lambda}x} \right)$$

where s is spin degeneracy. In formula Eq. (26) we have found useful to separate the contribution in absence of hybridization (first line of Eq. (26)) from a remainder (last line). Through the adiabatic potential we compute the phonon PDF as

$$(27) \quad P(x) = \frac{\exp(-\beta V(x))}{Z}.$$

Taking advantage of the Gaussian nature of the fermions we get for the local propagator

$$(28) \quad G(\omega) = \int dx P(x) \frac{1}{G_0^{-1}(\omega) - \sqrt{\lambda}x}.$$

which defines the self consistency condition through Eq. (6).

The self-consistency condition (6) together with Eqs. (28,27,26), completely solves the problem. Notice also the correspondence between the spinless and the spinful case upon rescaling λ to $\lambda/2$ in the latter case [15]. For the Bethe lattice (at zero temperature) it can be shown that the potential (26) becomes double well above a critical value $\lambda_{pot} = 3\pi/(8s)$. A MIT occurs at a larger coupling $\lambda_{MIT} = 1.328/s$ [15].

The BO procedure goes on by quantizing the adiabatic potential after adding the phonon kinetic energy contribution. Introducing the scaled variable $u = gx/\sqrt{s}$ the BO phononic Hamiltonian reads

$$(29) \quad H_{BO} = -\frac{\gamma}{2s} \frac{d^2}{du^2} + sV(u).$$

and $V(u)$ is given by Eq. (26). Notice that the spinful BO Hamiltonian maps onto twice the spinless one upon rescaling

$$(30) \quad \begin{aligned} \lambda/2 &\rightarrow \lambda \\ 2\gamma &\rightarrow \gamma. \end{aligned}$$

While phonon properties are immediately obtained at this stage from the solution of the one-dimensional anharmonic system of Hamiltonian Eq. (29), electronic properties must account non-trivially for the tunneling of phonon coordinates.

The simplest way to describe electrons coupled to a tunneling system is to map it onto a two level system. In our model this can be accomplished by changing the basis (operators a) from that of the harmonic oscillator to the that defined by the solution of (29). Then projecting out all the states but the first two ($|+\rangle, |-\rangle$) we get the following two state projected model (TSPM):

$$H = -\frac{2}{s} \sum_{\sigma} \epsilon \left(f_{\sigma}^{\dagger} f_{\sigma} - \frac{1}{2} \right) \sigma_z - \Delta \sigma_x + \sum_{k,\sigma} E_k c_{k,\sigma}^{\dagger} c_{k,\sigma} +$$

$$(31) \quad + \sum_{k,\sigma} V_k \left(f_{\sigma}^{\dagger} c_{k,\sigma} + c_{k,\sigma}^{\dagger} f_{\sigma} \right),$$

where σ_x and σ_z are two Pauli matrices in the space spanned by $|+\rangle$ and $|-\rangle$ and the quantities ϵ and Δ are given by

$$(32) \quad \epsilon = g \frac{s}{2} \langle + | a + a^{\dagger} | - \rangle$$

$$(33) \quad \Delta = \frac{\omega_0}{2} (\langle + | a^{\dagger} a | + \rangle + \langle - \rangle - | a^{\dagger} a | - \rangle)$$

The latter quantity Δ is the tunneling frequency between the two phononic states. A similar model has been introduced in Ref. [23] to study the strong coupling limit of the Holstein model. The TSPM reproduces exactly the DMFT of the Holstein model in two limits: weak coupling and adiabatic limit. In the former case the projection of the phonon space has no relevance therefore the TSPM reproduces the perturbation expansion developed (in the limit of infinite bandwidth) in Ref. [24]. The adiabatic limit is instead recovered as $\Delta \rightarrow 0$. No phonon tunneling occurs and the model can be solved exactly by CPA recovering the solution of Ref. [15].

To analytically span from the strong ($V_k \rightarrow 0$) to the weak ($g \rightarrow 0$) coupling regimes of the equivalent impurity Hamiltonian it is useful to devise an Iterated Born-Oppenheimer Coherent Potential Approximation (IBOCPA) scheme. Starting from the Green's function for $V_k = 0$ (35) for the spinless case and (36) for the spinful one, we notice that in both cases $G_a(\phi)$ can be written as sum of two contribution $G_a(\phi) = (1/2)(G_{a,+}(\phi) + G_{a,-}(\phi))$ where (\pm) label a phonon state [25]. Then we write the propagator in presence of hybridization as

$$(34) \quad G(\phi) = \frac{1}{2} \sum_{\alpha=\pm} \frac{1}{G_{a,\alpha}^{-1}(\phi) - \frac{D^2}{4} G(\phi)}$$

where the hopping of the electron from the impurity to the bath is described by the cavity-field correlator $D^2/4G(\phi)$ (6). Iteration proceeds substituting the propagator (34) back in Eq. 26 giving a new BO potential and new TSMP parameters (eq. (32)) and finally a new Green's function. Iteration continues after convergence is reached [26].

In (34) $G_{a,\alpha}^{-1}(\phi)$ are propagators obtained from the solution of the atomic ($V_k = 0$) limit of the TSPM in both spinless and spinful cases. The spinless atomic Green's function can be easily found to be

$$(35) \quad G_a(\phi) = \frac{1}{2} \sum_{\alpha=\pm} \left(\frac{\epsilon^2}{l^2} \frac{1}{\phi + 2l\alpha} + \frac{\Delta^2}{l^2} \frac{1}{\phi} \right)$$

$G_a(\omega)$ has a pole at $\omega = 0$ induced by phonon tunneling, whose weight vanishes as $\Delta \rightarrow 0$, accompanied by two resonances at $\pm 2l$. The zero energy peak is due to transitions in which both charge and phonon "spin" change while the side peaks arise from charge transfer in a frozen phonon "spin". In this sense the side peaks are adiabatic features which survive when phonon tunneling $\Delta \rightarrow 0$. The spinful atomic Green's function is

$$(36) \quad G_a(\phi) = \frac{1}{2} \sum_{\alpha=\pm} \frac{1}{2l} \left(\frac{l - \Delta}{\phi + \alpha(l + \Delta)} + \frac{l + \Delta}{\phi + \alpha(l - \Delta)} \right)$$

The most striking difference with the spinless case (35) is the absence of the zero frequency pole. In the spinful case the tunneling of the phonon Δ is always associated to a finite energy transition, and it only splits the finite frequency poles associated to the transition from singly to the empty or doubly occupied ones.

IBOCPA assumes that the tunneling states of the phonon in the adiabatic potential remain unaltered during an hybridization event. As in standard CPA a band is associated to each local level, but our IBOCPA gives a Fermi liquid solution in the spinless case for every value of the coupling, as opposed to the case of the Hubbard model. The low-energy band arising from the zero energy pole in the zero hybridization limit is indeed *coherent*. This can be easily realized by analysis of the self-energy. When $\omega \rightarrow 0$ the spinless propagator defined by (35) and (34) is dominated by the zero-energy pole of G_a (35) and consequently the self-energy obtained through (34) is purely real.

Conversely in the spinful case a MIT due to local pair formation occurs in the CPA approximation at a critical value of λ . Finally we emphasize that we recover the adiabatic solution of Ref. [15] as $\gamma \rightarrow 0$ for finite λ as $\Delta \rightarrow 0$. In this case the IBOCPA is exact and gives the Green's function of Ref. [15]. However the IBOCPA procedure is certainly affected by serious problems approaching the MIT in the spinful case. A more careful treatment of the low-energy part of the Green's function has been performed in this case in Refs. [23, 27, 1], where it has been observed a MIT scenario similar to the half-filled the Hubbard model, i.e., a quasi-particle peak that shrinks to zero width approaching a critical value of λ . In the spinless case instead a resonance is present at zero energy within a CPA approach. It is not associated to a Kondo effect but rather to phonon tunneling which drives charge fluctuations. On the other hand a Kondo like behavior can be ascribed to the bipolaron or pair formation. For a discussion of the limitation of the IBOCPA approach see also Ref. [25].

5.2. Antiadiabatic regime. – While in adiabatic limit the phonon displacement becomes a classical variable, and we are left with an electronic model which depends parametrically on it, in the opposite limit ($\gamma \gg 1$) the roles are exchanged, and we have a parametrically fixed electronic charge on a given site. In this regime the most reasonable starting point is the Lang-Firsov (LF) canonical transformation [28, 29] $S = \exp(T)$. The generator of the transformation reads

$$(37) \quad T = -\alpha \sum_{\sigma} (f_{\sigma}^{\dagger} f_{\sigma} - \frac{1}{2})(a^{\dagger} - a),$$

introducing the parameter $\alpha = g/\omega_0$ which is the relevant e-ph coupling parameter in the anti-adiabatic regime [30, 8].

The canonical transformation diagonalizes the impurity Hamiltonian in the absence of hybridization by eliminating the e-ph interaction part. In the spinful case the phonon energy term of (14) gives rise to the well known bipolaronic instantaneous attraction [29]. The hybridization term of (14) is modified by acquiring an exponential term in the phonon coordinates leading to

$$(38) \quad e^T H e^{-T} = - \sum_{k,\sigma} e^{\alpha(a^{\dagger}-a)} V_k (c_{k,\sigma}^{\dagger} f_{\sigma} + h.c.) + \sum_{k,\sigma} E_k c_{k,\sigma}^{\dagger} c_{k,\sigma} - 2 \frac{g^2}{\omega_0} (s-1) n_{\uparrow} n_{\downarrow} - \frac{g^2}{\omega_0} \sum_{\sigma} (\frac{1}{2} - n_{\sigma}) + \omega_0 a^{\dagger} a,$$

where $n_\sigma = f_\sigma^\dagger f_\sigma$. Notice that in the anti-adiabatic limit $\gamma \rightarrow \infty$, if λ is kept constant α vanishes. In this case spinless electrons are not renormalized, while spinful electrons are described by an attractive Hubbard model with $|U|/D = \lambda$.

If we want to proceed with analytical methods, the hybridization term must be treated in an approximate way. Assuming that in the anti-adiabatic limit the impurity density is constant during the fast motion of the phonon, we average out the phonon term on the displaced phonon ground state. This is the so-called Holstein Lang-Firsov Approximation (HLFA), which has not to be confused with the exact canonical transformation (37). HLFA gives rise to the exponential renormalization of the hybridization constants where each V_k is replaced by $V_k \exp(-\alpha^2/2)$. Such a replacement implies the well known exponential renormalization of the bandwidth $D \exp(-\alpha^2)$.

To get the *electron* Green's function $G(\omega)$, the explicit action of LF transformation have to be taken into account into both creation and destruction operators appearing in the definition of the Green function. Following Refs. [31] and [32], we obtain in both spinless and spinful cases

$$(39) \quad G(\omega) = e^{-\alpha^2} G_p(\omega) + \frac{1}{2} \sum_{n \neq 0} e^{-\alpha^2} \frac{\alpha^{2|n|}}{|n|!} G_p(\omega - n\omega_0).$$

where $G_p(\omega)$ is the Green's function of an impurity (with a negative U interaction in the spinful case) with an exponentially reduced hybridization to a bath of conduction electrons. The self-consistency condition can be written explicitly in the spinless case due to the lack of interaction terms on the impurity:

$$(40) \quad G_p(\omega) = \frac{1}{\omega - e^{-\alpha^2} \frac{t^2}{4} G(\omega)}.$$

where $G(\omega)$ is the local Green's function of the lattice. In the spinful case a Lang-Firsov Coherent Potential Approximation (LFCPA) can be devised for the resulting HLFA attractive Hubbard model with $U = -2g^2/\omega_0$ giving

$$(41) \quad G_p(\omega) = \frac{1}{2} \left(\frac{1}{\omega - e^{-\alpha^2} \frac{t^2}{4} G(\omega) - U/2} + \frac{1}{\omega - e^{-\alpha^2} \frac{t^2}{4} G(\omega) + U/2} \right).$$

Notice that the theory developed here for the Holstein impurity model differs from that developed directly in the lattice model[31]. In that case an equation identical to (39) is recovered for a band of free electrons therefore giving a low-energy *coherent* polaronic band in the spinless case. It is however easy to show that this form of the spectral function is not compatible with a k -independent self-energy. The self-consistency condition (40) gives rise to a non-zero damping at the Fermi level even in the spinless case. However, when γ becomes larger α gets smaller reproducing the anti-adiabatic coherent behavior at low energy in the spinless and the negative- U behavior in the spinful cases.

In the anti-adiabatic regime the HLFA approach gives an estimate of the MIT

$$(42) \quad \lambda_{MIT} = |U/D|_{MIT} \exp(-\alpha^2)$$

where $|U/D|_{MIT} \simeq 2.94$ is the MIT value of the negative- U Hubbard model [33]. The pairing MIT occurs for smaller λ as the adiabatic regime is approached (see Fig. 5).

The phonon PDF can be easily derived within LF approach. Being the local electron densities parametric variables in the anti-adiabatic we find

$$(43) \quad P(x) = \sum_l w_l P_0(x - x_l)$$

where w_l is the probability of having an occupancy n_l , x_l the relative displacements and $P_0(x)$ the ground state PDF of an harmonic oscillator. $P_0(x - x_l)$ is then the conditional probability of having a displacement x given a definite occupation n_l . In the spinless case $n_l = 0, 1$ with equal probability giving

$$(44) \quad P(X) = \frac{1}{2} (P_0(x - x_0) + P_0(x + x_0))$$

where $x_0 = \sqrt{\lambda}/2$. A definite polarization can be associated to the ground state if the PDF becomes bimodal. By requiring $dP(X)/dX|_{X=0} > 0$, which simply means $X = 0$ turns from a maximum to a minimum, we get the usual anti-adiabatic condition for the existence of a polaronic state, i.e., $\alpha^2 > 1$ (see fig. 5).

In the spinful case $n_l = 0, 1, 2$

$$(45) \quad P(X) = n_d(P_0(X - 2X_0) + P_0(X + 2X_0)) + (1 - 2n_d)P_0(X)$$

where $n_d = \langle n_\uparrow n_\downarrow \rangle$ is the site double occupancy. It is worth noting that in the insulating state $n_d \simeq 1/2$, and the zero-displacement PDF associated to singly occupied sites is depleted. The existence of a definite polarization is now associated to a bipolaronic state. The condition under which (45) becomes bimodal, is

$$(46) \quad \exp(-2\alpha^2)(4\alpha^2 - 1) \geq \frac{1 - 2n_d}{2n_d}.$$

An estimate for the bipolaronic transition can be obtained by taking $n_d = 1/2$, which gives $\lambda_{pol} = \gamma/2$. The presence of a fraction of singly occupied states increase the critical value of λ (see Fig. 5). We notice that the spinful PDF for $n_d = 1/2$ maps onto the spinless one after the *same rescaling* of the adiabatic regime (30).

5.3. Results from DMFT-ED. – The behavior of $P(x)$ and ρ obtained from DMFT-ED compared with that of the previous theories is shown in Figs. 3 and 4 for adiabatic and antiadiabatic regime respectively. In each diagram the value of the quantity shown has been shifted upward according to the value of the coupling lambda. The values of γ and λ have been chosen according to the scaling (30).

Let us first discuss the adiabatic regime. Polaron crossover is seen as a qualitative change in the shape of phonon PDF shown in the upper panels of Fig. 3 where BO approximation and DMFT results are compared. The anharmonicity due to e-ph interaction increases as the coupling increases leading first to a non-Gaussian and finally to a bimodal PDF at $\lambda > \lambda_{pol}$. This behavior signals the appearance of static distortions, even if we are neglecting any ordering between them. From Fig. 3 is evident that BO approximation works well in *both* the metallic and the polaronic regimes. The reason for the accuracy of the BO procedure in the polaronic regime is that, contrary to its usual implementation in the weak e-ph coupling[34], here we take into account

the anharmonicity through Eq. (29) in a non perturbative way. However, BO does not accurately reproduce the phonon PDF around the polaron crossover. In this case electron and phonon states are strongly entangled, and cannot be approximated properly by a disentangled BO state. By a comparison of the spinless and spinful cases in Fig. 3 we see that the occurrence of the MIT does not influence much the differences between full DMFT and BO, which are in both cases relevant near the polaron crossover. In the lower panels of Fig. 3 we compare the electronic DOS from ED-DMFT with IBOCPA. The different behavior of the spinless and spinful case is not so evident. However, comparing the spinless spectrum with the corresponding spinful, we see that a quasiparticle peak is present in the former case, while a depletion of low energy part is much more evident in the latter. At strong coupling the discretization of the bath inherent to the ED solution of DMFT does not allow us to identify a well defined quasiparticle peak in the spinless case. A more careful analysis of the quasi particle spectral weight [35] shows however that no pairing MIT occurs in the spinless case. Notice that the IBOCPA seems to be much closer to DMFT-ED in the spinless than in the spinful case where the CPA approximation for the electronic degree of freedom is apparently much less adequate.

The upper panel of Fig. 4 shows that the phonon PDF becomes bimodal at a very large value of the coupling. HLFA overestimates polaronicity in the spinless case while it behaves better in the spinful case. In the lower panels of Fig. 4 the electron DOS is compared with the results of HLFA in the antiadiabatic regime. The different behavior of spinless and spinful cases is marked here by the presence of a pairing MIT in the former, well before the (bi)polaron crossover. HLFA correctly catches the gross behavior of the DOS. Notice that at the strong coupling the CPA employed to obtain the lower diagrams accurately reproduces both the position and the width of the side bands.

The different behavior of spinless and spinful system can be easily understood in terms of strong coupling anti-adiabatic perturbation theory for the original lattice problem [36] introducing the charge sector pseudo-spins [37]. In the spinful case at second order in hybridization V_k an anisotropic Kondo Hamiltonian can be obtained [38, 39, 25]. The anisotropic Kondo couplings (see also Eq. (8) of Ref.[40]) reads

$$(47) \quad J_{\parallel,\perp} = \frac{8V^2}{D} \sum_m (\pm)^m \frac{e^{-\alpha^2} \alpha^{2m}}{m!(m\gamma + \lambda/2)},$$

where the $+$ ($-$) sign is taken for the \parallel (\perp) coupling and we have assumed for simplicity $V = \sum_k V_k$. In the spinless case the processes leading to J_{\perp} do not exist while the remaining J_{\parallel} is solely associated to charge fluctuations. As opposed to the charge Kondo effect of the spinful case, no Kondo effect is expected for spinless fermions. A strong coupling estimates of J_{\parallel} gives

$$(48) \quad J_{\parallel} \simeq \frac{8V^2}{D\lambda}$$

and $J_{\perp}/J_{\parallel} \propto \exp(-2\alpha^2)$ which means an exponential suppression of the superconductivity versus charge correlation at strong coupling due to retardation effects [38, 39]. In the anti-adiabatic limit $\gamma \rightarrow \infty$ instead the Kondo couplings becomes isotropic.

The above observations can be summarized in the phase diagrams of Fig. 5. The polaron crossover line λ_{pol} is strongly γ dependent in both cases. Above this line a polaronic (bipolaronic) regime is attained in the spinless (spinful) case. In the spinful case, we also have a λ_{MIT} line, which separates a normal phase from a paired insulating

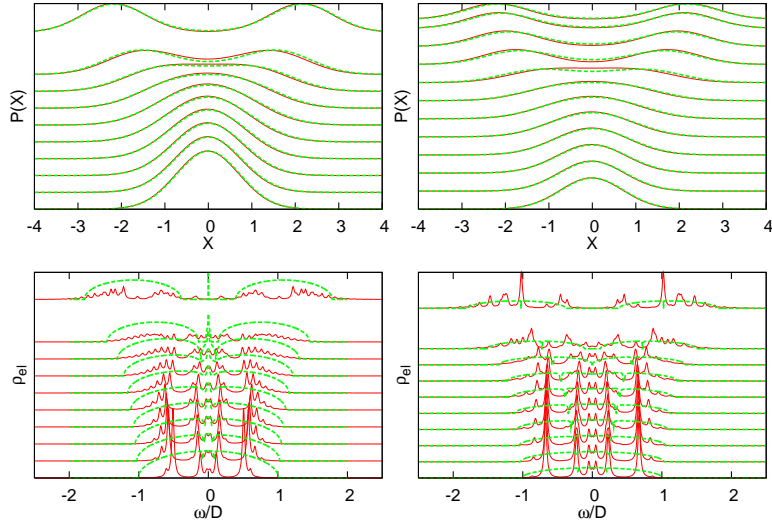


Fig. 3. – DMFT data in the adiabatic regime $\gamma = 0.1$ spinless (panels on the left) and $\gamma = 0.2$ spinful (panels on the right). The various curves refer to different value of λ spanning from 0.1 to 1.8 in the spinless case and from 0.05 to 1.1 in the spinful case and are shifted according λ value. Upper panels show the phonon PDF while lower panels the electronic DOS.

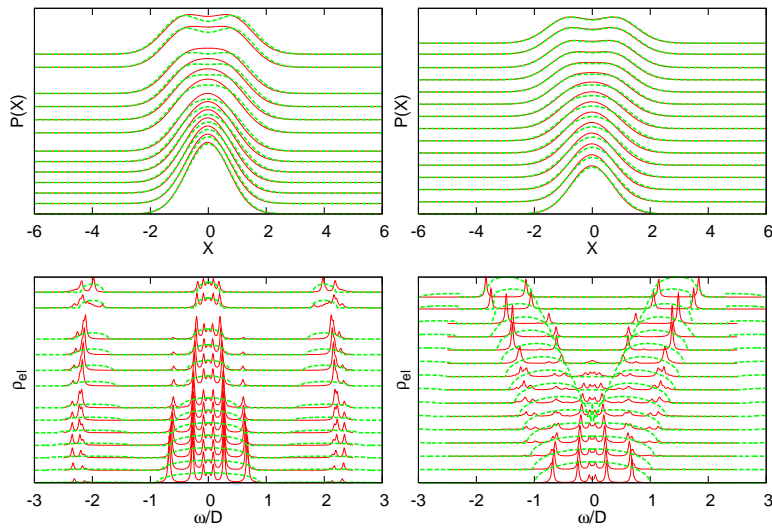


Fig. 4. – DMFT data in the antiadiabatic regime $\gamma = 2.0$ spinless (panels on the left) and $\gamma = 4.0$ spinful (panels on the right). The various curves refer to different value of λ spanning from 0.4 to 6.5 in the spinless case and from 0.2 to 3.0 in the spinful case and are shifted according λ value. Upper panels show the phonon PDF while lower panels the electronic DOS.

phase[35]. For large phonon frequency we can have pairs without bipolaronic behavior, as it can be understood by recalling that in the antiadiabatic limit the Holstein model becomes an attractive Hubbard model, where no polarization is associated to the pairing.

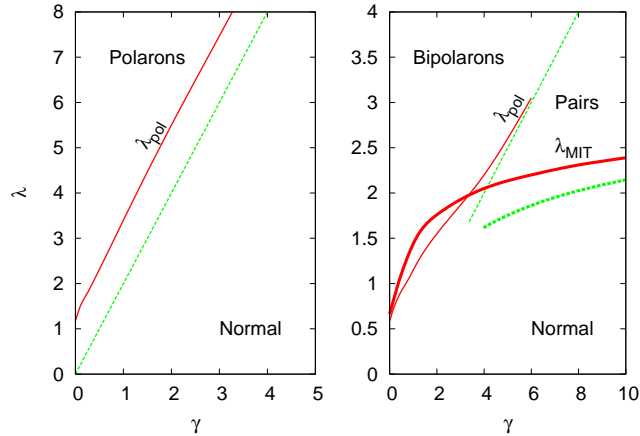


Fig. 5. – Phase diagrams of the spinless (left) and spinful (right) $T = 0$ Holstein model at half filling. Left panel: the bold line is the polaron crossover from bimodality of $P(x)$ and the dotted line is the anti-adiabatic estimate $\lambda_{pol} = 2\gamma$ for the polaron crossover. Right panel: bold curve is the bipolaronic MIT from vanishing of quasi-particle spectral weight Z , thin solid line the polaron crossover, bold dotted line is the anti-adiabatic prediction for bipolaronic MIT (Eq. (42)), light dotted line is the anti-adiabatic estimate $\lambda > \gamma/2$ for the polaron crossover.

6. – Half filled Holstein model: spinless vs spinful cases at $T > 0$

Using the QMC procedure described in section 3.1 we are able to study the normal phase at finite temperature. At fairly high temperature the MIT becomes a crossover and we are faced with the problem of finding a suitable quantity to locate unambiguously this crossover. In analogy with the phonon PDF used to mark the polaron crossover we can define a distribution of a quantity that locates the pairing crossover. Let us define the distribution of the center of mass X_c (“centroid”) of the phonon path

$$(49) \quad P(X_c) = \left\langle \delta\left(X_c - \frac{1}{\beta} \int_0^\beta x(\tau) d\tau\right) \right\rangle$$

where the averages are evaluated over the action (11-13). In the same formalism the phonon PDF is the distribution of the the endpoint $x = x(0) = x(\beta)$.

The meaning of the centroid variable X_C has been discussed in [41] for a single particle in a binding potential. Here the variable X represents the fluctuating position of the particle, and X_c is the classical position of the particle [41]. For an heavy particle, the classical limit holds, so that $P(X)$ and $P(X_C)$ coincide [41]. The lighter is the particle, the broader the wave function, increasing the variance of $P(X)$ while $P(X_C)$ turns out to be essentially determined by the binding range of the potential. Here, we use $P(X_C)$ for the many-body problem, and propose that pairing can be associated with

a multimodal behavior in $P(X_c)$ which takes place at a given value of the coupling λ_{pair} . [42] The ability of our estimator to determine the pairing crossover can be understood by inspecting the interaction term (13). In the adiabatic limit ($\gamma \rightarrow 0$) the kinetic term forces the phonon path to be τ -independent and the phonon field becomes classical. In this limit X_c is equal to X and $P(X)$ and $P(X_c)$ obviously coincide. Thus the centroid distribution becomes bimodal when the system is polarized, i.e., $\lambda_{pair} = \lambda_{pol}$, which is exactly what one expects since a static field can induce pairing only with a finite polarization. Notice that in this sense the bimodality of $P(X_c)$ is a *precursor* of the actual pairing MIT which occurs at $T = 0$ and $\omega_0 = 0$ at a *larger* value of the coupling [15] (see fig. 5).

On the other hand, in the opposite atomic ($D \rightarrow 0$, $\gamma \rightarrow \infty$) limit the electron density becomes a constant of motion. Therefore Eq. (13) takes the transparent form $-\sqrt{\lambda}(n-1) \int_0^\beta d\tau x(\tau)$ where the electron density is directly coupled to the centroid X_c . The average appearing in Eq. (49) is readily carried out, giving

$$(50) \quad P(X_c) \propto \exp \left[-\beta \left(\frac{X_c^2}{2} - \frac{1}{\beta} \log(2 \cosh(\beta \sqrt{\lambda} X_c + 1)) \right) \right]$$

which becomes bimodal for $\lambda > \lambda_{pair} = 2T$. This is exactly the scale where double occupancies start to proliferate in the atomic limit. Therefore the bimodality of $P(X_c)$ correctly signals the onset of pairing also in the antiadiabatic regime. In the same limit, it can be proved that the endpoint distribution $P(X)$ has a variance which scales with $1/\sqrt{\Delta\tau}$ and as a consequence no definite polarization may occur. We finally notice that the $D \rightarrow 0$ limit of adiabatic $P(x)$ [15] coincides with $P(X_c)$ of Eq. (50). Since for $\omega_0 = 0$ the distributions of X and X_c coincide, we conclude that in the atomic limit $P(X_c)$ is the same for $\omega_0 = 0$ and $\omega_0 = \infty$. This suggests that the pairing crossover may depend on ω_0 more weakly than the polarization one.

6.1. Results from DMFT-QMC. – To analyze the evolution of $P(X)$ and $P(X_c)$ at finite D and ω_0 we use DMFT-QMC. The numerically exact results, shown in Fig.6, clearly show that $P(X)$ and $P(X_c)$ tend to coincide in the relatively adiabatic case $\gamma = 0.1$, as expected from the previous arguments about the adiabatic limit. The two quantities are clearly different for $\gamma = 1$ and 8. For temperatures smaller than ω_0 , the polarization crossover λ_{pol} moves to larger values as γ is increased, while the line (λ_{pair}) where $P(X_c)$ becomes bimodal is only slightly shifted to larger couplings with increasing γ . This is strongly reminiscent of the behavior of the metal-insulator transition in the Holstein model at $T = 0$, whose critical coupling is slowly increasing with γ and then saturates to the asymptotic $\gamma = \infty$ value[35]. The polarization crossover is instead roughly proportional to γ [35]. Both at zero and at finite temperature the line where the centroid becomes bimodal does not coincide with the metal-insulator line, but it can be considered a precursor which depends in a very similar way on γ and on λ .

Our DMFT results can also be compared with the semi-analytical results for $\gamma = 0$ [15] (thin dashed line in Fig.6). The $\gamma = 0.1$ case is in very good agreement with the adiabatic result, and also the $\gamma = 1$ and 8 cases, at high temperature, fall on the same curve. The centroid distribution depends weakly on γ , as suggested by the atomic limit. Interestingly, the adiabatic result displays a re-entrance at low temperatures as a non monotonic behavior of λ_{pair} and λ_{pol} as a function of temperature. Although the QMC simulations do not reach sufficiently low temperatures, we find that the re-entrance is

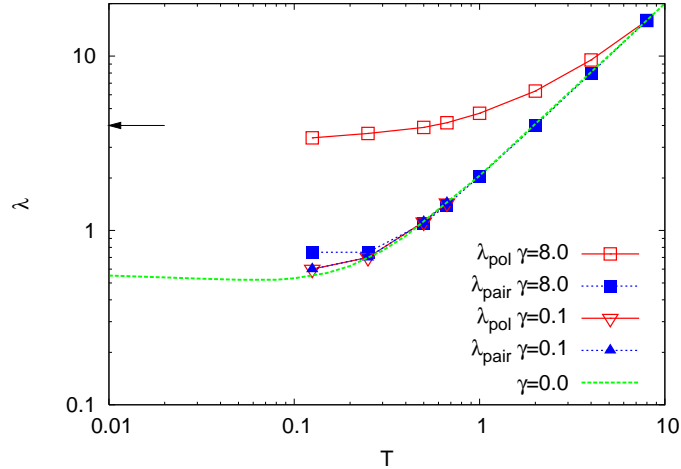


Fig. 6. $-\lambda_{pair}$ and λ_{pol} at $\gamma = 8$. The dashed line represents the $\gamma = 0$ result where $\lambda_{pair} = \lambda_{pol}$. The dashed arrow indicates the zero-temperature results for the polaron crossover λ_{pol} for $\gamma = 8$.

present also for γ different from zero, as indicated by the arrows in Fig.6, which mark $T = 0$ results for the polarization crossover for the Holstein model[35].

7. – Conclusions

The normal state properties of strongly coupled electron phonon systems can be drawn from the comparison of electronic spectral and phonon PDF properties.

Qualitative changes in phonon PDF signals a polaronic crossover while an electronic MIT can be seen from a gap in the electronic DOS or by the vanishing of the quasi particle spectral weight. This last transition can be observed only at sufficiently high density provided the Coulomb repulsion is neglected. In the limit of low density the carrier show a polaronic behavior trough developing a definite polarization in the phonon PDF while at large densities occupied and empty sites makes the phonon PDF bimodal. At the polaron crossover fluctuation of phonon coordinates tends to be larger than those at any other coupling. In this regime Born-Oppenheimer approximation is shown to fail also when phonon frequency is much less then electron bandwidth. For a single hole in the $t - J$ model a further source of localization is due to magnetic superexchange energy which tends to localize the spin-defect spreading due to the presence of the hole.

At non zero temperature the pairing MIT becomes a crossover. To locate the point of this crossover it is possible to define a suitable distribution associated to the phonon classical position which is coupled to the electron density in the non-adiabatic regime.

There are several limitations in the DMFT method used to obtain the present results. The biggest one is the non dispersive nature of bosonic excitation. In the $t - J$ case the absence of spin-wave dispersion lead to localization of the single hole. However local properties seem to be quite well represented by DMFT in when compared with those found at finite dimensions [9]. In the half filled Holstein model case bipolarons do not have coherent motion therefore the vanishing of the single particle spectral weight implies a MIT. Several extensions of DMFT such as Extended-DMFT for the $t - J$ model [43]

or CDMFT for the Hubbard model [44] try to overcome such limitations. Work along these lines for the Holstein and Holstein-Hubbard model are currently in progress.

REFERENCES

- [1] HEWSON A C, *This volume editor please update page*, ()
- [2] CASTELLANI C., *This volume editor please update page*, ()
- [3] EGAMI, *This volume editor please update page*, ()
- [4] CALVANI P, *This volume editor please update page*, ()
- [5] FEHSKE H, ALVERMANN A, *This volume editor please update page*, ()
- [6] S. FRATINI AND F. DE PASQUALE, S. CIUCHI, *Phys. Rev. B*, **63** (2001) 153101
- [7] H. SUMI *et al.*, *J. Phys. Soc. Japan*, **36** (1974) 770
- [8] S.CIUCHI, F.DE PASQUALE, S. FRATINI, AND D.FEINBERG, *Phys. Rev. B*, **56** (1997) 4494
- [9] MISHCENKO A, *This volume editor please update page*, ()
- [10] U. BRANDT C. MIELSCH, *Z. Phys. B*, **75** (1989) 365 ;
ibid **79** 1990 295;
U. BRANDT, A. FLEDDERIJORANN AND G. HÜLSEMBECK, *ibid* 81 1990 409 ;
U. BRANDT C. MIELSCH, *ibid* 82199137
- [11] E.MULLER-HARTMANN, *Z.Phys. B*, **74** (1989) 507
- [12] A. GEORGES, *et al.*, *Rev. Mod. Phys.*, **68** (1996) 13
- [13] ORLAND H., NEGELE J.W., “*Quantum Many Particle Systems*”, (Addison Wesley, Redwood City) 1988.
- [14] R.BLANKENBECLER, D. J.SCALAPINO, AND R. L. SUGAR, *Phys. Rev. D*, **24** (1981) 2278
- [15] A.J.MILLIS, R. MUELLER AND B. I. SHRAIMAN, *Phys. Rev. B*, **54** (1996) 5389
- [16] V.S. VISWANATH AND G. MÜLLER, “*The Recursion Method*”, (Springer-Verlag) 1994
- [17] FEHSKE H, BRONOLD F X, AND ALVERMANN A, *This volume editor please update page*, ()
- [18] E. CAPPELLUTI AND S. CIUCHI, *Phys. Rev. B*, **66** (2002) 165102
- [19] G. MARTÍNEZ AND P. HORSCH, *Phys. Rev. B*, **44** (1991) 317
- [20] R. STRACK AND D. VOLLHARDT, *Phys. Rev. B*, **46** (1992) 13852
- [21] This expression is equivalent to the CPA free energy of the Kimball Falikov model [10, 22]
- [22] WOOKI CHUNG AND J. K. FREERICKS, *Phys. Rev. B*, **57** (1998) 11955
- [23] P. BENEDETTI, R. ZEYER, *Phys. Rev. B*, **58** (1998) 14320
- [24] S. ENGELSBERG AND J.R. SCHRIEFFER, *Phys. Rev.*, **131** (1963) 993
- [25] M. CAPONE, P. CARTA, S. CIUCHI, *cond-mat/0509542*, (2005)
- [26] Notice that in contrast with ref.[25] here iteration to adjust TSMP parameter is fully implemented.
- [27] D. MEYER, *et al.*, *Phys. Rev. Lett.*, **89** (2002) 196401
- [28] I. G. LANG AND YU. A. FIRSOV, *Sov.Phys. JETP*, **16** (1963) 1301
- [29] RANNINGER J, *This volume editor please update page*, ()
- [30] M. CAPONE, W. STEPHAN, AND M. GRILLI, *Phys. Rev. B*, **56** (1997) 4484;
M. CAPONE, C. GRIMALDI, AND S. CIUCHI, *Europhys. Lett*, **42** (1998) 523
- [31] JULIUS RANNINGER, *Phys. Rev. B*, **48** (1993) 13166
- [32] A. S. ALEXANDROV AND J. RANNINGER, *Phys. Rev. B*, **45** (1992) 13109;
A. S. ALEXANDROV AND J. RANNINGER, *Physica C*, **198** (1992) 360
- [33] M. CAPONE, C. CASTELLANI, AND M. GRILLI, *Phys. Rev. Lett.*, **88** (2002) 126403;
A. TOSCHI, P. BARONE, M. CAPONE, AND C. CASTELLANI, *New Jour. of Phys.*, **7** (2005) 7
- [34] E.G. BROVMAN AND YU. KAGAN, *Sov. Phys. JETP*, **25** (1967) 365
- [35] M. CAPONE, S. CIUCHI, *Phys. Rev. Lett.*, **91** (2003) 186405
- [36] J. K. FREERICKS, *Phys. Rev. B*, **48** (1993) 3881
- [37] R. MICNAS, J. RANNINGER, AND S. ROBASZKIEWICZ, *Rev. Mod. Phys.*, **62** (1990) 113-171
- [38] P.S. CORNAGLIA, H. NESS, AND D.R. GREMPPEL, *cond-mat* 0409021, (2004)

- [39] G. SANGIOVANNI, M. CAPONE, C. CASTELLANI, AND M. GRILLI, *Phys. Rev. Lett.*, **94** (2005) 026401
- [40] P.S. CORNAGLIA, H. NESS, AND D.R. GREMPEL, *Phys. Rev. Lett.* *93*, **2004** (147201)
- [41] H. KLEINERT, “*Path Integrals in Quantum Mechanics Statistics and Polymer Physics*”, (World Scientific, Singapore) 1995 2nd ed
- [42] S. CIUCHI, G. SANGIOVANNI, M. CAPONE, [cond-mat/0503681](#), (2005)
- [43] K. HAULE A. ROSCH, J. KROHA AND P. WOLFLE, *Phys. Rev. B*, **68** (2003) 155119
- [44] M. CIVELLI, M. CAPONE, S.S. KANCHARLA, O. PARCOLLET, AND G. KOTLIAR, *Phys. Rev. Lett.*, **95** (2005) 106402